Accurate hyper-Rayleigh scattering polarization measurements

David P. Shelton
Department of Physics and Astronomy, University of Nevada, Las Vegas, Nevada 89154-4002, USA

(Received 29 August 2011; accepted 16 October 2011; published online 4 November 2011)

Apparatus and methods are described for measurement of the polarization dependence of hyper-Rayleigh scattering near 90° scattering angle with 0.1% accuracy for all four configurations where the incident and scattered light is linear polarized either parallel or perpendicular to the scattering plane. Measurements are made with large collection aperture and extrapolated to zero collection numerical aperture ($NA = 0$). Fiber coupling allows the system to be easily reconfigured for either polarization or spectral measurements. © *2011 American Institute of Physics*. [doi:10.1063/1.3658481]

I. INTRODUCTION

Hyper-Rayleigh scattering (HRS) is second-harmonic light scattering mediated by the molecular first hyperpolarizability β, and HRS is widely employed to measure β of organic chromophores in solution.[1–8] It is usually assumed that the molecules are independent and randomly oriented, so that the observed HRS signal from the sample is the result of incoherent addition of HRS from each individual molecule. Tensor components of β are obtained from experimental measurements of the HRS intensity and its polarization dependence.[3–5] With linearly polarized incident and scattered light only two invariants are measurable (in the case where Kleinman symmetry holds), and no additional information is obtained by departing from the 90° scattering geometry.[9] However, up to six invariants of the β tensor are accessible by HRS in the most general case, and recent work has explored the use of other scattering angles and elliptical polarization states of the incident and scattered light to measure all six invariants.[10,11] Recent work has also addressed the need to measure the frequency dependence of β by developing apparatus which combines broad spectral tunability of the input laser and spectral analysis of the HRS light.[7,8]

The present apparatus was developed to enable very accurate HRS polarization measurements with linear polarized light at or near the 90° scattering geometry. The motivation for such measurements is the finding that the polarization and angular dependence of HRS from some molecular liquids is inconsistent with the assumption of independent randomly oriented molecules.[12–14] The unexpected molecular correlations are most clearly revealed by measurements of linear polarized HRS at 90° scattering angle. The usual 90° scattering configurations with incident and scattered light polarized either perpendicular or parallel to the horizontal scattering plane are denoted VV, HV, VH, and HH, where V denotes vertical polarization, H denotes horizontal polarization, and the first and second letters refer to the incident and scattered light, respectively. The observation $I_{HV} \neq I_{VH}$ for the HRS intensities is inconsistent with independent randomly oriented molecules, and the present apparatus was developed to facilitate study of the long range polar molecular correlations revealed by this observation.

II. EXPERIMENTAL APPARATUS

The apparatus may be configured for either HRS polarization or spectral measurements as shown in Figure 1. Linearly polarized pulses from an injection-seeded single-longitudinal-mode Nd:YAG (yttrium aluminum garnet) laser (operating at $\lambda = 1064$ nm, 4.3 kHz repetition rate, 100 ns pulse duration, 3 MHz spectral bandwidth, full width at half maximum [FWHM]) are focused into the liquid sample contained in a 10 mm rectangular fused silica fluorometer cuvette. Light scattered near the 90° scattering angle is collected and collimated by a lens, analyzed by a polarizer, focused by another lens into an optical fiber, and fiber coupled to spectral filters and the photon counting detector. The intensity of the laser beam is adjusted by rotating a half-wave retardation plate (HWP) placed before a fixed Glan-laser calcite prism polarizer (POL). The polarization state of the laser beam incident on the sample is controlled using a liquid crystal variable wave plate (LCVWP, Meadowlark Optics) following the prism polarizer (subsequent depolarization by the optics and cuvette windows is negligible), and any light near the second harmonic wavelength is removed by a Schott RG-780 short wave absorptive glass filter. The collected and analyzed HRS light from the sample is ultimately detected by a cooled photon-counting photomultiplier tube (PMT) with a GaAsP(Cs) photocathode (Hamamatsu H8631-40). A 532 nm interference filter (60 cm^{-1} FWHM, 90% peak transmission, Semrock), a KG3 infrared blocking filter, and any required neutral density filters (F) are inserted in the collimated beam between the two relay lenses that couple the output of the final optical fiber to the photocathode. A fiber-coupled dual etalon (DE, 0.3 cm^{-1} FWHM) may also be inserted to reduce the spectral range for the detected light.

There are two modes of operation for the apparatus. In the first mode, the linear polarization state of the laser beam produced by the LCVWP and the linear polarization state selected by the analyzing polarizer are switched in a coordinated fashion while recording the photon counts for each setting (Fig. 1(a)). For example, the apparatus may alternately measure the photon counts with the apparatus set for the HV and VH polarization configurations. Rapidly alternating measurements are averaged to reduce the effect of drifts and

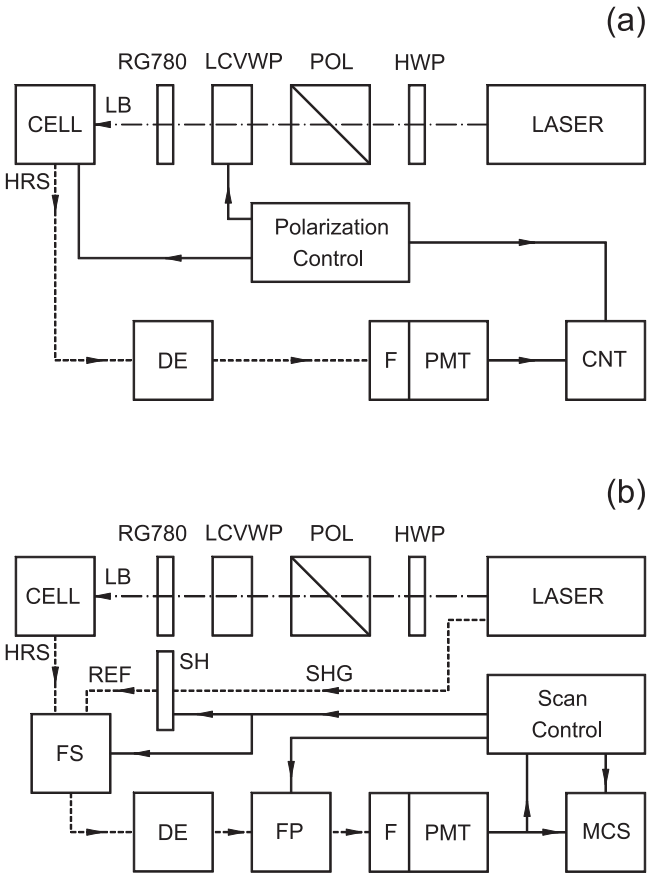

FIG. 1. Configuration of the apparatus for (a) polarization or (b) high resolution spectral measurements. Optical fiber and electronic connections are shown by dashed and solid lines, respectively. The laser beam (LB, dot-dash line) is prepared using the half wave plate (HWP), prism polarizer (POL), liquid crystal variable wave plate (LCVWP), and long wave pass filter (RG780) before being focused into the sample in the scattering cell assembly (CELL). In (a) the output light (HRS) from the sample cell assembly is sent through the selected filters (DE, F) to the detector (PMT), and the polarization controller synchronizes the switching of the LCVWP, analyzing polarizer (in CELL), and the photon counting electronics (CNT). In (b) the fiber switch (FS) transmits either HRS or REF light to the scanning confocal Fabry-Pérot (FP) interferometer and the spectral data is accumulated in the multichannel scaler (MCS). The scan controller synchronizes the operation of the reference shutter (SH), FS, FP, and MCS, and also generates a feedback signal during the REF spectral scan that is used to stabilize the FP scan with respect to the frequency of the second harmonic light (SHG) from the laser.

fluctuations in laser power, alignment, and mode (typically 10^2–10^4 repeats).

In the second mode of operation (Fig. 1(b)), the polarization configuration is fixed (e.g., VH) and the HRS spectrum is measured using a fiber-coupled hermetic-sealed scanning confocal Fabry-Pérot interferometer (FP, 750 MHz free spectral range, 10 MHz FWHM resolution). This measurement is needed to assess the contribution to the HRS spectrum due to dissolved ions.[13–15] Multiple scans by the Fabry-Pérot are synchronized with the scans by the multichannel scaler (MCS) that records the photon counts and displays the spectrum. The run time to acquire a spectrum is typically several hours, so the Fabry-Pérot is stabilized using a feedback signal generated by scanning the spectrum of the second harmonic (SHG) light generated from the laser beam by a potassium titanyl phosphate crystal. The HRS spectrum and the SHG reference spectrum are recorded on alternate scans of the Fabry-Pérot, using a fiber switch (FS) to direct light from either the HRS or the reference (REF) fiber to the detector fiber. The scan controller also closes a shutter (SH) to block the reference light except when the reference is selected by the fiber switch. The fiber switch uses a 45° prism that rotates between two mirror-symmetric minimum deviation orientations to deflect the collimated beam from the selected input port to the output port (switch time < 0.1 s). The polarization dependence due to oblique incidence on the prism is compensated by a fixed glass plate placed before the output port of the fiber switch and tilted around an axis orthogonal to both the output beam and the prism rotation axis.

Figure 2(a) shows the scattering cell and collection optics. A lens (L1, $f = 16$ mm) focuses the 3 mm diameter laser beam (LB) to an 8 μm diameter beam waist in the sample cuvette (CUV). (A thermal lens in the sample due to absorption at the 1064 nm laser wavelength will result in a larger waist diameter and lower HRS signal, and is usually eliminated with a deuterated sample.) The waist is located 5 mm from the entrance window of the 10 mm cuvette, and 1.6 mm behind the viewing window. Light is collected and collimated by an aspheric lens (L2, $f = 4$ mm, $NA = 0.62$) (NA denotes numerical aperture), the light polarization is analyzed by a dichroic linear polarizer (DP, 1×10^{-4} extinction ratio, 90% transmission, 0.2% reflection, Meadowlark Optics), and the light is then focused by another aspheric lens (L3, $f = 11$ mm, $NA = 0.25$) into the core of a step-index multimode optical fiber (200 μm core diameter, $NA = 0.22$) at the HRS output port of the collection optics assembly. The aperture stop (AS) controlling the numerical aperture of the collection optics is an iris placed in the collimated beam 1.5 mm after the second vertex of the collection lens L2.

Mechanical details of the construction of the collection optics assembly are shown in Figure 2(b). The sample cuvette is pressed securely into an inside corner of the temperature controlled aluminum holder by a nylon tip set screw, and the collection lens L2 is mounted at a fixed position on the holder. The cuvette holder and collection optics assembly is mounted on a rotation stage and stacked x-y-z translation stages, while the laser focusing lens L1 is mounted on separate translation stages and does not move with the collection optics assembly. The incidence angle of the laser beam on the cuvette is adjusted by rotating the cuvette using the rotation stage, and the focal point of collection lens is centered on the laser beam waist by translating the entire cuvette and collection optics assembly. Slots in the holder allow access for the focused laser beam, and a hole on the side opposite the collection lens allows the scattering region to be imaged and viewed by a charge coupled device (CCD) camera.

The iris that forms the aperture stop is carried in a cylindrical plug with a conical tapered nose that matches the 5.5° taper of the socket in the lens mount for L2, as shown in Fig. 2(c). The iris is a circular hole cut into a 0.050 mm thick stainless steel foil disk pressed into the 6 mm diameter cylindrical pocket in the nose of the plug. The hole in the foil is cut using the beam from the HRS measurement laser at 3 W average power, focused to a 36 μm beam waist diameter using a $f = 75$ mm lens. A block with a tapered hole matching the

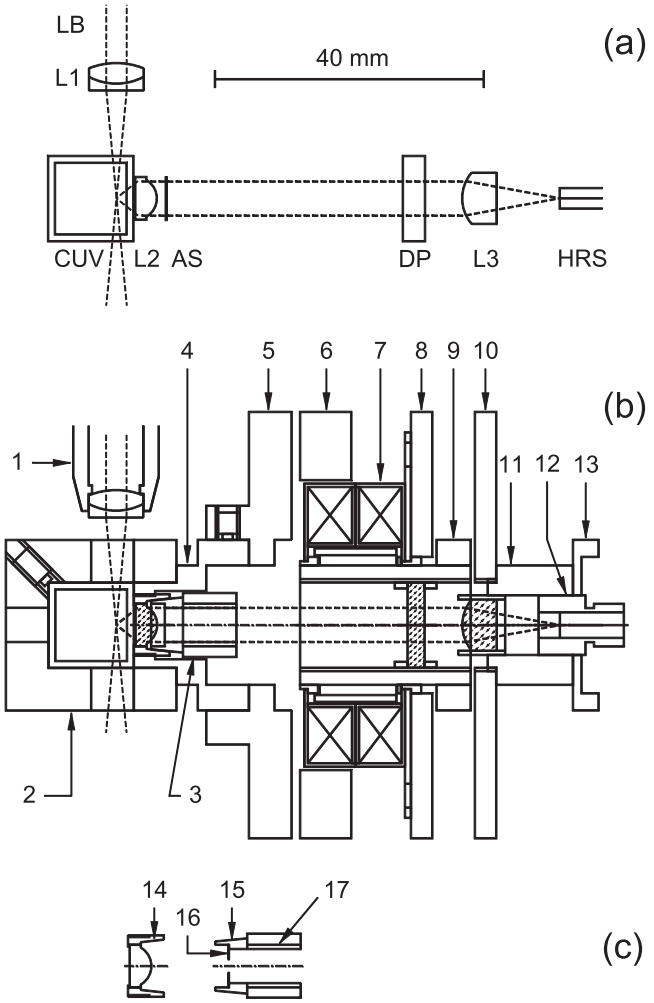

FIG. 2. (a) Top view of the optical components in the scattering cell assembly. The laser beam (LB) is focused by a lens (L1) into the sample cuvette (CUV), and the scattered light is collected and collimated by an aspheric lens (L2), with *NA* set by the aperture stop (AS). The collimated beam transmitted through the dichroic polarizer (DP) is focused by another aspheric lens (L3) into the optical fiber at the output port (HRS). (b) Cross section showing mechanical details of the scattering cell assembly. The main components are the laser focus lens mount (1), cuvette holder (2), collection lens and iris plug (3), collection lens mounting collar (4), rotatable support disk with angle scale on rim (5), ring with tilt adjusters and magnetic coupling to the support disk (6), motor body (7), motor mounting plate (8), motor rotor and fiducial ring (9), fiber lens mounting plate (10), threaded barrel (11), SMA fiber socket with focus adjust thread (12), and focus lock ring (13). (c) Cross section showing the taper socket (14) in the collection lens mount, and the matching taper nose (15), iris disk (16), and extraction thread (17) in the iris plug.

taper of the iris plug is mounted behind the cuvette holder, the position of the block is adjusted using the x-y-z stage so that the foil will lie at the focus of the laser beam, the plug carrying the foil is inserted into the taper, and the laser beam is unblocked. Rotating the taper plug in the matching taper socket cuts a circular hole in the foil that is precisely centered on the axis of the conical taper, with the diameter determined by the offset between the laser beam axis and the taper axis (the hole is circular and centered within 2 μm). Pressing the plug carrying this iris into the socket of the collection lens mount precisely and reproducibly centers the iris on the axis of L2 (0.014°/μm collection axis shift due to iris decentering). The collection *NA* is adjusted using a set of interchangeable iris plugs with different diameter irises (a screw inserted into the threaded body of the plug serves as a handle to remove the plug from the socket when interchanging iris plugs).

The cylindrical collar holding L2 extends from the side of the cuvette holder, and slips into a socket in the disk which supports the remaining components. The disk has an angular scale engraved on its rim, and it is rotated on the collar to align the analyzing polarizer axis, and then is fixed with nylon-tip set screws. There is a kinematic tilt adjustment and magnetic coupling between this disk and the ring carrying the remaining components. The disk has a flat pad, V-groove, and conical hole that engage the spherical tips of three fine-thread adjustment screws mounted in the facing ring, and the disk and ring are held together by the attraction of four pairs of NdFeB magnets (6 mm long, 6 mm diameter). The disk and ring can be disconnected to allow access to the iris plug, and then reconnected without disturbing the alignment of the optic axis. The ring carries both the motor that rotates the polarizer between precise V and H orientations (switch time < 0.1 s),[16] and the fiber-coupling lens L3 and SMA output fiber socket (with M9-0.5 focus adjustment thread).

III. ALIGNMENT AND CALIBRATION

The scattering geometry is defined using the surface of the optical table as the horizontal reference plane and a pair of triangular optical benches placed on the table along the incident and 90° scattering directions. A convenient alignment tool is obtained by coupling some of the 532 nm SHG beam from the laser into a single mode (SM) optical fiber and collimator. The collimated beam from this tool is set parallel to the first optical bench, and the second optical bench is set at 90° to the first bench using the 90° deflected beam produced by inserting a pentaprism. To establish the absolute azimuth for the input polarization the pentaprism is repositioned so the beam is incident on the first surface at Brewster's angle and reflected in the horizontal plane. H polarization for the incident beam is obtained by rotating the preceding prism polarizer to extinguish this reflection, and V polarization is obtained by a further 90° rotation of the polarizer. The analyzing polarizer in the collection arm is set to H polarization by sending the collimated V polarized 532 nm beam (pentaprism removed) into a cuvette filled with a dilute suspension of 0.1 μm polystyrene spheres to produce V polarized scattered light, then rotating the analyzing polarizer to minimize the transmitted signal. Adjusting the orientation of the cuvette so that the incident beam is retroreflected will set the input face of the cuvette at normal incidence. At the collection optics HRS output port, the fiber end face is set at the focus of the fiber coupling lens by inserting the SM fiber into the HRS port and adjusting the SMA socket position to produce a collimated beam. Then, with lens L2 removed, the optic axis of the fiber coupling optics is set to the 90° scattering direction using the tilt adjustment screws in the collection arm to point the collimated beam parallel to the second optical bench. The final alignment of the collection axis is made with L2 and a 0.050 mm iris installed, so that the light travelling backwards through the collection optics exits as a 0.7° diameter

cone centered on the actual collection axis. A small tilt adjustment aligns the axis of this cone in the 90° direction.

Several adjustments must be made using the main 1064 nm laser beam. First, the 0 and 1/2 wave settings of the LCVWP for the 1064 nm beam are determined using extinction of the transmitted beam from the LCVWP by a second prism polarizer set for V or H polarization. Second, the laser focus lens L1 is precisely centered on the 1064 nm beam using a four-quadrant Si photodiode detector (4QD) placed after the cuvette holder. The 4QD is centered on the laser beam with L1 removed, and then L1 is replaced and its position adjusted until the beam spot is again centered on the 4QD. The last adjustment is the final focusing of the collection optics, done every time the sample cell or the scattering angle is changed. The x-y-z stages are used to place the focal point of the collection lens on the laser beam waist, so that the image of the scattering source is centered on the 200 μm core of the output optical fiber with 3 μm precision. The scattering angle and the incident and scattered polarization angles obtained using the above procedures are accurate to better than 0.1°.

The typical HRS signal is much less than one photon count per laser pulse, but in some cases the signal is much stronger and one laser pulse may produce several detected photons closely bunched near the peak of the laser pulse. Inaccurate results due to the high instantaneous count rate are avoided by having the first detected photon trigger an electronic pulse wider than the duration of the laser pulse, so that the electronics registers either a count of zero or one for each laser pulse. The true count rate $\tilde{S}$ is determined from the measured signal count rate S by applying the expression $\tilde{S} = -R\ln(1 - S/R)$, where R is the laser pulse repetition rate, and Poisson counting statistics are assumed.[17] For $\tilde{S}/R \leq 1$ the measured error for $\tilde{S}$ is less than 0.1%. An electronic gate that only accepts photon counts during the laser pulse reduces the background count rate to 10^{-3} count/s.

Calibration of the instrument relative response for different polarizations is done using the unpolarized two-photon fluorescence (2PF) from a 5×10^{-4} M solution of disodium fluorescein in D_2O.[13] This calibration source is bright, convenient, and reliable since HRS and 2PF sources have nearly the same spatial distribution and dependence on laser beam parameters.[13,18] The calibration factor $c_1 = (I_{VH}/I_{HH})_{2PF}$ for the input arm is measured by switching the LCVWP, and the calibration factor $c_2 = (I_{HV}/I_{HH})_{2PF}$ for the collection arm is measured by switching the analyzing polarizer. The polarization dependent transmission of the LCVWP (due to larger liquid crystal director fluctuations and scattering at low applied voltage) accounts for the factor $c_1 = 1.003$ measured with the beam normally incident on the cuvette. This result agrees with direct laser beam transmission measurements for the LCVWP made with a thermal power meter. The reflection at the cuvette entrance face also becomes polarization dependent as the cuvette is rotated away from normal incidence, which reduces c_1 by about 0.1% for a 4° rotation. The calibration factor $c_2 = 1.001$ at normal incidence is found to be independent of *NA*, increases 0.1% for a 4° rotation of the cuvette, and changes 3%/mm when the source image is moved across the face of the output fiber. The final focusing is done with the same V analyzing polarizer orientation for both the 2PF and HRS sources to avoid a possible systematic error in the calibration due to this position sensitivity. The common path for all polarization signals contributes to the 0.1% stability observed for the instrument calibration.

IV. EXPERIMENTAL RESULTS AND DISCUSSION

HRS polarization ratios measured for deuterated nitrobenzene ($C_6D_5NO_2$, Isotec, 99.5 atom% D) with $T = 25.0$ °C, $\theta = 90°$, 0.9 W average laser power, and 60 cm^{-1} spectral bandwidth (DE removed) are shown in Figure 3. Each data point is the result of 300–4000 alternating measurements of 10 s duration (1–11 h acquisition time), with the HRS signal attenuated to stay in the range 100–3000 count s^{-1}. Aperture stops with nominal diameter 1.0, 1.5, 2.0, 3.0, and 4.0 mm were used for the measurements, and the collection *NA* (0.124, 0.187, 0.249, 0.375, and 0.500) was determined from the actual measured aperture diameter and a ray trace of the optics. The HRS intensity ratios are extrapolated to $NA = 0$ by fitting functions linear in $(NA)^2$ to the data for the four smallest apertures (solid lines), with the

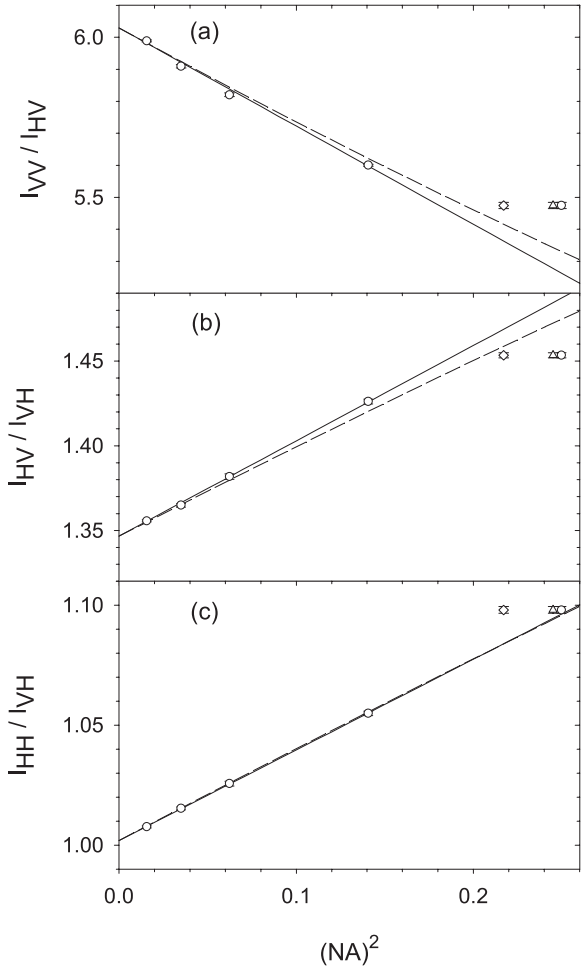

FIG. 3. Extrapolation to $NA = 0$ for measurements of the HRS polarization ratios (a) $I_{VV/HV}$, (b) $I_{HV/VH}$, and (c) $I_{HH/VH}$ for $C_6D_5NO_2$. The solid lines are empirical fits to the first four of the data points (open circles), while the dashed curves are based on a theoretical model. Alternative *NA* estimates for the largest aperture give the data points plotted as open triangles and diamonds.

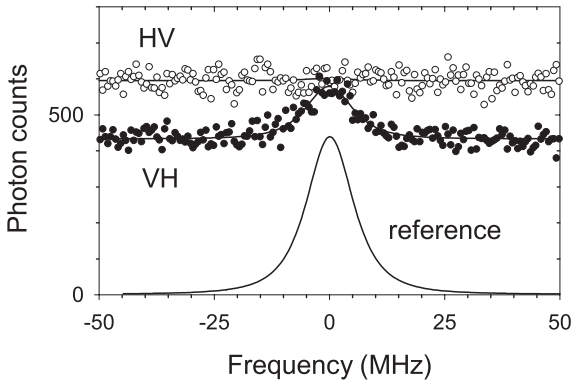

FIG. 4. Fabry-Pérot scan data are shown for the VH (filled circles) and HV (open circles) HRS spectra for $C_6D_5NO_2$. The solid curves show the instrumentally broadened SHG reference spectrum and the fits to the VH and HV HRS spectral data. The longitudinal polar mode induced by dissolved ions in the sample produces the characteristic instrumentally broadened spike seen in the high resolution VH HRS spectrum but absent from the HV HRS spectrum. The spike/background integrated intensity ratio *S*/*B* determined from the high resolution VH HRS spectrum is used to assess and correct for the ion contribution to the HRS signal.

results $I_{VV}/I_{HV} = 6.029 \pm 0.006$, $I_{HV}/I_{VH} = 1.3467 \pm 0.0006$, and $I_{HH}/I_{VH} = 1.0017 \pm 0.0007$. The error bars shown on the points in Figure 3 are about ±0.1% and are based on photon counting statistics only. The error contributions due to laser fluctuations and calibration uncertainties will be comparable or larger when the HRS photon count rate exceeds about 500 count s^{-1}, and the resulting excess scatter of the points around the fit lines is taken into account in assessing the uncertainties for the extrapolated polarization ratios. The deviation from $I_{HH}/I_{VH} = 1$ indicates that the actual scattering angle is $\theta = 90.06^\circ \pm 0.03^\circ$ instead of 90°.[13]

Figure 4 shows the high resolution HV and VH HRS spectra for the $C_6D_5NO_2$ sample and the laser SHG reference spectrum (2.0 mm aperture stop, DE removed, 20 h acquisition time). The curves fit to the HRS spectra are the sum of the scaled SHG reference peak (13 MHz FWHM) and a constant background term. The relative integrated intensity of the spike and the broad background in the VH spectrum is $S/B = 0.0068 \pm 0.0006$ (as compared to 0.0002 ± 0.0005 for the HV spectrum). Correcting for the intensity of the VH spike due to ionic contamination gives $(I_{HV}/I_{VH})_{corr} = (I_{HV}/I_{VH})(1 + S/B) = 1.3559 \pm 0.0010$ for pure nitrobenzene-d5. The large deviation from $I_{HV}/I_{VH} = 1$ indicates the presence of strong long range polar molecular correlations. The above results are consistent with results from previous experiments.[13,18]

Typical HRS measurements use a collection aperture as large as $NA = 0.6$ (angular diameter 74°), and the *NA* dependence of the polarization ratios is either ignored or theoretical corrections are applied to the measured ratios.[2–5,19,20] An exception is the extrapolation of polarization ratio measurements made over the range $NA = 0.08$–0.56 by Wong *et al.*[21] In the present work, extrapolation to zero *NA* is done with the fewest theoretical assumptions by using simple empirical fit functions which adequately represent the data except for the measurements with the largest aperture. The theoretical model developed in Ref. 13 gives approximately the same *NA* dependence as the data and the empirical fit (model adjusted to agree at $NA = 0$, dashed curves in Figure 3), but the theoretical model assuming independent random molecular orientation cannot be made to agree with the I_{HV}/I_{VH} data in Figure 3.

The polarization ratio data points obtained with the largest aperture do not fall on the curves in Figure 3, which could indicate a problem with the *NA* value calculated from the iris diameter. Therefore, the effective *NA* was also estimated photometrically in two ways, using a fiber-coupled incandescent (QTH) light source and miniature integrating sphere, or using the 2PF source. All three *NA* estimates agree for each of the four smaller irises, but not for the largest iris. Data points for the largest iris are plotted with all three *NA* values in Figure 3. The effective *NA* estimated using the integrating sphere (triangles) is close to the value calculated from the measured iris diameter (circles), but the effective *NA* estimated using the 2PF source (diamonds) is smaller. This result is expected for the sharply localized 2PF source since both the optical coupling into the core of the output fiber and the effective *NA* will be reduced due to image aberrations (which are a strong function of aperture size). However, no choice of *NA* for the largest aperture forces all the data to agree with the fit lines, which brings into question the reliability of polarization ratios obtained by applying theoretical corrections to measurements made at large *NA*.

The sharp spike in the VH HRS spectrum for nitrobenzene-d5 seen in Figure 4 is the result of dissolved ions with a concentration about 10^{-6} M.[22] In other samples, the intensity of this contribution can be much larger, especially for solvents such as water in which ionic salts readily dissolve and dissociate.[15] Ionic contaminants are removed very effectively from liquids such as water, methanol or acetonitrile, which are compatible with ion exchange resin (Dowex Monosphere MR-450 UPW), by circulating the liquid in a loop containing the deionizing resin column, particle filter, sample cell, conductivity cell, reservoir, and peristaltic pump (PTFE tubing). An alternative for sufficiently volatile liquids is to distil the sample directly into the cuvette (this is less effective but also requires less sample liquid). In weakly polar or non-polar liquids such as $CHCl_3$ or CCl_4 ionic contaminants do not dissociate and are not a problem. In any case the strategy is to reduce the ion concentration if possible, then measure and correct for the residual effect.

Sample liquids are usually passed through a 0.2 μm particle filter to remove dust, and the cleanliness of the sample is conveniently assessed using a CCD camera to view the focused laser beam in the sample. Compared to other apparatus,[4] the HRS measurements with the present apparatus are relatively insensitive to dust in the sample. This is a consequence of the low peak power of the 100 ns laser pulses, which allows the beam to be more tightly focused in the sample. The sensitive volume of the sample is the intersection of the focused laser beam with the viewed volume of the collection optics, a cylinder 8 μm diameter and 70 μm long, with volume 4×10^{-6} mm^3. This small sensitive volume greatly reduces the probability for viewing a dust particle. The tight focusing also results in a beam spot diameter 0.6 mm at the cuvette windows, which reduces the laser beam intensity there

and helps prevent window damage. The focusing of the laser beam has a negligible effect on the scattering geometry since the mean square slope of the laser beam wavefronts in the sensitive volume is 100× smaller than the mean square slope of the collected wavefront for the smallest (1.0 mm) collection aperture.

The HRS measurement apparatus and techniques presented above allow accurate polarization ratio measurements using a precisely defined scattering geometry and rapid polarization switching. Stability of the calibration is a result of the common path for the signals, and extrapolation to zero *NA* gives the polarization ratio at a particular scattering angle instead of the average over a large angular range. The apparatus can be reconfigured to make high resolution spectral measurements that are needed to distinguish clearly the HRS contribution induced by dissolved ions, so that polarization ratios intrinsic to the pure liquid can be obtained. Fiber coupling simplifies reconfiguration of the apparatus. The sensitivity of the apparatus permits measurements for a wide range of liquids and solutions.

[1]K. Clays and A. Persoons, Phys. Rev. Lett. **66**, 2980 (1991).
[2]K. Clays and A. Persoons, Rev. Sci. Instrum. **63**, 3285 (1992).
[3]G. J. T. Heesink, A. G. T. Ruiter, N. F. van Hulst, and B. Bolger, Phys. Rev. Lett. **71**, 999 (1993).
[4]I. D. Morrison, R. G. Denning, W. M. Laidlaw, and M. A. Stammers, Rev. Sci. Instrum. **67**, 1445 (1996).
[5]P. Kaatz and D. P. Shelton, J. Chem. Phys. **105**, 3918 (1996).
[6]C. H. Wang, Y. C. Lin, O. Y. Tai, and A. K.-Y. Jen, J. Chem. Phys. **119**, 6237 (2003).
[7]J. Campo, F. Desmet, W. Wenseleers, and E. Goovaerts, Opt. Express **17**, 4587 (2009).
[8]J. Zhu, C. Lu, Y. Cui, C. Zhang, and G. Lu, J. Chem. Phys. **133**, 244503 (2010).
[9]R. Bersohn, Y. Pao, and H. L. Frisch, J. Chem. Phys. **45**, 3184 (1966).
[10]M. Kauranen and A. Persoons, J. Chem. Phys. **104**, 3445 (1996).
[11]V. Ostroverkhov, R. G. Petschek, K. D. Singer, L. Sukhomlinova, R. J. Twieg, S.-X. Wang, and L. C. Chien, J. Opt. Soc. Am. B **17**, 1531 (2000).
[12]D. P. Shelton, J. Opt. Soc. Am. B **17**, 2032 (2000).
[13]D. P. Shelton, J. Chem. Phys. **132**, 154506 (2010).
[14]D. P. Shelton, J. Chem. Phys. **133**, 234507 (2010).
[15]D. P. Shelton, J. Chem. Phys. **130**, 114501 (2009).
[16]D. P. Shelton, W. M. O'Donnell, and J. L. Norton, Rev. Sci. Instrum. **82**, 036103 (2011).
[17]D. P. Shelton, Phys. Rev. A **42**, 2578 (1990).
[18]J. Chen and K. Y. Wong, J. Chem. Phys. **122**, 174505 (2005).
[19]P. Kaatz and D. P. Shelton, Rev. Sci. Instrum. **67**, 1438 (1996).
[20]S. Brasselet and J. Zyss, J. Opt. Soc. Am. B **15**, 257 (1998).
[21]S. W. Wong and K. Y. Wong, Opt. Commun. **133**, 268 (1997).
[22]D. P. Shelton, J. Chem. Phys. **129**, 134501 (2008).